



## Removal of Sunset Yellow dye using heterogeneous catalytic degradation with magnetic Fe<sub>3</sub>O<sub>4</sub>/persulfate/ultrasound system

Afshin Takdastan<sup>a,b</sup>, Sudabeh Pourfadakari<sup>b,c,\*</sup>, Nader Yousefi<sup>d,\*</sup>, Naghmeh Orooji<sup>e</sup>

<sup>a</sup>Environmental Technologies Research Center, Ahvaz Jundishapur University of Medical Sciences, Ahvaz, Iran, email: afshin\_ir@yahoo.com (A. Takdastan)

<sup>b</sup>Department of Environmental Health Engineering, Ahvaz Jundishapur University of Medical Sciences, Ahvaz, Iran

<sup>c</sup>Student Research Committee, Ahvaz Jundishapur University of Medical Sciences, Ahvaz, Iran, email: porfadakar@gmail.com (S. Pourfadakari)

<sup>d</sup>Department of Environmental Health Engineering, School of Public Health, Tehran University of Medical Sciences, Tehran, Iran, email: yousefinader@gmail.com (N. Yousefi)

<sup>e</sup>Department of Environmental Engineering, College of Agriculture and Natural Resources, Ahvaz Branch, Islamic Azad University, Ahvaz, Iran, email: n.oroji2007@gmail.com (N. Orooji)

Received 26 August 2019; Accepted 9 April 2020

### ABSTRACT

Azo dyes with a complex aromatic structure released into the environment by various industries and make the main concern for humans. In this study, nanoparticles of magnetic Fe<sub>3</sub>O<sub>4</sub> were synthesized with co-precipitation method and employed as an activator for persulfate (PS) for degradation of Sunset Yellow (SSY) molecules in the presence of ultrasound irradiation (US). Decolorization tests were carried out as a control test with different processes (Fe<sub>3</sub>O<sub>4</sub>, Fe<sub>3</sub>O<sub>4</sub>/PS, Fe<sub>3</sub>O<sub>4</sub>/PS/US, zero-valent iron (ZVI)/PS/US, US, and PS). Adsorption study before the oxidation experiments showed that the maximum adsorption occurred at an initial 30 min and then reached the equilibrium at 60 min. In addition, the oxidation experiments revealed that the maximum degradation rate was obtained at acidic pH, 0.4 g/L of catalyst dose and 4 mM of persulfate so that at a reaction time of 120 min, 97.4% of dye with the initial concentration of 20 mg/L was removed. The effect of various anions showed that anions especially carbonate acted as a radical scavenger and decreased the degradation of dye molecules. Also, the enhancement factor ( $R = 1.08$ ) indicated that the synergetic effect that occurred at Fe<sub>3</sub>O<sub>4</sub>/PS/US system and catalytic activity can critically affect the removal rate of SSY. The Fe<sub>3</sub>O<sub>4</sub>/PS/US system as a promising method could be considered as an efficient and effective technique for the degradation of dye molecules of wastewater.

*Keywords:* Dye degradation; Mineralization; Magnetic nanoparticles; Adsorption; Catalytic oxidation

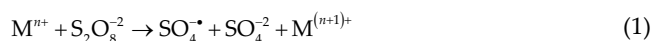
### 1. Introduction

Synthetic dyes can be produced and released into the environment by various industries such as textiles, paper, food and pharmaceutical, and leather and cause concern for the environment and human health [1,2]. Azo dyes have a complex aromatic structure, which has been widely used for

different purposes, these types of dyes can be recognized with two nitrogen atoms (N=N) and create allergy, skin irritation and enhance mutation and cancer in human beings [3,4]. The individual structure of these dyes causes them to make them non-biodegradable in aerobic treatment and generate more hazardous compounds in anaerobic treatment [5,6]. Therefore, these compounds should be removed from

\* Corresponding authors.

aqueous solutions with appropriate techniques [7]. In the last years, many methods have been taken for dye removal from aqueous solutions. These techniques are adsorption, advanced oxidation processes (AOPs), photocatalysis, coagulation, and chemical oxidation and membrane filtration [3,8]. These methods suffer from some disadvantages such as inefficiency for removing pollutants completely, expensive, and unavailability in some areas [9]. Adsorption can be considered as a single, easy operating, and cost-effective process for the treatment of dye wastewater. [10]. Among adsorbents such as natural zeolite and activated carbon, magnetic nanoparticle due to having characteristics such as large surface area and high reactivity have been widely used for pollutant purification. A combination of new adsorbent with strong oxidants could enhance the activation of the persulfate (PS) and degradation of resistant compounds [11]. There are many experiences about the application of the oxidation process for dye removal. AOPs can accelerate the degradation of toxic and recalcitrant contaminants with the generation of reactive hydroxyl ( $\text{HO}^\bullet$ ) and other radicals. Persulfate ( $\text{S}_2\text{O}_8^{2-}$ ) is a strong oxidant, which redox potential of it is 2.01 V [12–14]. This oxidant is quickly decomposed and generates sulfate radical which redox potential of it is 2.6 V and has a long lifetime (30–40  $\mu\text{s}$ ) and higher selectivity for the oxidation of contaminants, that can degrade most of the organic compounds from aqueous solution at wide pH range. Mostly, persulfate can activate with various methods like transition metals, heat, heterogeneous catalysts, and UV irradiation according to Eqs. (1)–(3) [11,12].



There are many studies, which investigate the effect of transitional metals on the activation of persulfate. Iron is a special transitional metal among other metals due to it is naturally abundant, low expenses, and environmentally friendly [11,15]. On the other hand,  $\text{Fe}^{2+}$  could rapidly convert to  $\text{Fe}^{3+}$  and cause to enhance the reaction rate and radical production because divalent iron could consume the sulfate radical and consequently decrease the oxidation efficiency [13]. Therefore,  $\text{Fe}_3\text{O}_4$  as a nanoparticle was used to accelerate radical production as a novel approach. In this study, the effect of  $\text{Fe}_3\text{O}_4$  as an adsorbent and  $\text{Fe}_3\text{O}_4$  in combination with persulfate and persulfate/ultrasound (US) was investigated. Moreover, the effect of competitive anions, scavenger, recovery of adsorbent, mineralization, and kinetic and isotherm study was studied.

## 2. Material and methods

### 2.1. Materials

Iron(II) chloride tetrahydrate ( $\text{FeCl}_2 \cdot 4\text{H}_2\text{O}$ ) and Iron(III) chloride hexahydrate ( $\text{FeCl}_3 \cdot 6\text{H}_2\text{O} \geq 98.0\%$ ), sodium hydroxide ( $\text{NaOH}, \geq 98.0\%$ ), hydrogen peroxide ( $\text{H}_2\text{O}_2, 35\%$ ), hydrochloric acid ( $\text{HCl}, \geq 98.0\%$ ), ethanol and the other chemicals

were purchased from Merck (Darmstadt, Germany). Sunset Yellow FCF (SSY) (96% purity, molecular weight 452.36 g/mol, formula:  $\text{C}_{16}\text{H}_{10}\text{N}_2\text{Na}_2\text{O}_7\text{S}_2$ ), was provided from Alvan Sabet Company, Hamadan, Iran. All chemicals were analytical grade and used without further purification.

### 2.2. Synthesis of magnetite nanoparticle ( $\text{Fe}_3\text{O}_4$ )

$\text{Fe}_3\text{O}_4$  magnetic nanoparticles were synthesized based on the co-precipitation method. In this method, ferric and ferrous salts were used in the presence of nitrogen gas. Summery,  $\text{FeCl}_2 \cdot 4\text{H}_2\text{O}$ , and  $\text{FeCl}_3 \cdot 6\text{H}_2\text{O}$  with a molar proportion of 1:2 (0.6 and 1.17 g, respectively) were dissolved at deionized water and agitated for 60 min at 70°C. Then,  $\text{NaOH}, 2 \text{ M}$  was added to the mixture and agitated as vigorous stirring for 30 min in the presence of  $\text{N}_2$  gas to achieve chemical precipitation (final pH:10) [16,17]. The resulted precipitates were separated with an external permanent magnet and washed several times with deionized water and ethanol solution. Ultimately, magnetic iron nanoparticles ( $\text{Fe}_3\text{O}_4$ ) were dried at 60°C overnight in the oven. The synthesis reaction of nanoparticles could be presented as Eq. (4) [17]:



### 2.3. Characterization of $\text{Fe}_3\text{O}_4$

The crystal structure of magnetic nanoparticles was determined using X-ray diffraction (XRD) analysis with (model PW1730, Philips, Holland). The region of  $2\theta$  range for analysis was 10° to 70° with the  $\text{Cu K}\alpha$  radiation ( $\lambda = 1, 54051 \text{ \AA}$ ). The size and morphology of nanoparticles were recorded with field emission-scanning electron microscopy (FE-SEM) (model Mira III, TESCAN, Czech Republic). Infrared spectra were employed for determining the molecular structure of magnetic nanoparticles through Fourier-transform infrared (FTIR) spectroscopy (AVATAR, USA). The surface area was determined with Brunauer–Emmett–Teller (BET, model: BELSORP MINI II, Japan). Energy-dispersive X-ray spectroscopy (EDS) analysis was applied for determining the composition of adsorbent and the magnetic property of nanoparticle was provided with vibrating sample magnetometers (VSM, model MDKFD, Iran).

### 2.4. Experiments

All experiments were done at room temperature ( $25^\circ\text{C} \pm 2^\circ\text{C}$ ) and batch system including the glass flasks with 250 mL, which was contain the 100 mL sample. The adsorption tests were carried out with a variety of effective factors pH (3–10), initial dye concentration (5–50 mg/L),  $\text{Fe}_3\text{O}_4$  nanoparticle (0.2–0.6 g/L) and contact time (0–60 min). The pH of the solution was adjusted with the addition of  $\text{HCl}$  (0.1 M) and  $\text{NaOH}$  (0.1 M). The mixture was agitated at 250 rpm for achieving the uniform solution. In addition, the oxidation process in the presence of a catalyst ( $\text{Fe}_3\text{O}_4$ ) was done at 250 rpm to provide a uniform mixture of reagent and solution. Samples were regularly withdrawn

from oxidation reactors at a given interval time, quenched with  $\text{Na}_2\text{S}_2\text{O}_3$  (0.2 M) quickly, and consequently analyzed to determine the residual of dye concentration. The concentration of persulfate oxidation at all experiments was between 0.5 to 6 mM. During the experiments, ultrasound power with 200 W was irradiated to the solution. Also, the effect of competition anions (nitrate, sulfate, chloride, and carbonate), and scavenger (ethanol) was investigated on the removal of dye. In addition, the results of this study ( $\text{Fe}_3\text{O}_4/\text{PS}/\text{US}$ ) was compared with the  $\text{Fe}_3\text{O}_4/\text{H}_2\text{O}_2/\text{US}$  process. Decolorization tests were carried out as a control test with different processes ( $\text{Fe}_3\text{O}_4$ ,  $\text{Fe}_3\text{O}_4/\text{PS}$ ,  $\text{Fe}_3\text{O}_4/\text{PS}/\text{US}$ , zero-valent iron (ZVI)/PS/US, US, and PS). Finally, the recovery and mineralization tests were done at optimum conditions.

The recovery tests were conducted at optimum conditions on the  $\text{Fe}_3\text{O}_4$  nanoparticle for four steps. The catalyst was separated from the mixture after each step, then washed with distilled water and was dried for used at the next step. The removal efficiency of dye was computed according to Eq. (5):

$$\text{Removal efficiency (\%)} = \left[ \frac{C_0 - C_t}{C_0} \right] \times 100 \quad (5)$$

where  $C_0$  and  $C_t$  refer to initial dye concentration and dye concentration at time  $t$ , respectively. To determine the maximum of adsorption wavelength by the dye in this study, the adsorption spectrum of dye, in dye concentration of 100 mg/L, and the wavelength range 200–600 nm by spectrophotometer UV/Vis (DR-6000 HACH model, USA) was investigated. In this experiment, it observed that the maximum absorption spectrum was in the visible area (400 nm). So, the wavelength of 400 nm was selected as the maximum wavelength.

### 2.5. Mineralization tests

Mineralization test was carried out based on the degradation of total organic carbon (TOC). TOC was measured using a TOC analyzer (Shimadzu  $V_{\text{CHS/CSN}}$ , Japan). The mineralization rate was done at the optimum condition of the oxidation process [1].

### 2.6. Isotherm and kinetic study

The most important models for the evaluation of kinetic (pseudo-first-order and pseudo-second-order model) and isotherm (Langmuir and Freundlich model) were evaluated for achieving the optimum condition of the adsorption process.

## 3. Results and discussion

### 3.1. Catalyst characteristics

Fig. 1a shows the XRD pattern of  $\text{Fe}_3\text{O}_4$  nanoparticles. The peaks of nanoparticles ( $2\theta$  value) were changed from  $0^\circ$  to  $70^\circ$ . The peaks of  $30.37^\circ$ ,  $31.9^\circ$ ,  $35.62^\circ$ ,  $43.44^\circ$ ,  $45.7^\circ$ ,  $57.3^\circ$ , and  $62.7^\circ$  could be contributed to 319.4; 885.4; 1,220.7; 321.9; 5,513; 334.5 and 447.7 and inverse cubic spinel structure of magnetic nanoparticles, respectively. These results were similar to previously found data for magnetic  $\text{Fe}_3\text{O}_4$

nanoparticles [18]. The sharp and good peaks of  $\text{Fe}_3\text{O}_4$  indicated that the nanoparticles synthesized were appropriately crystallized and were in a narrow size distribution [16].

FE-SEM could characterize the morphology and size of magnetic nanoparticles. Based on the FE-SEM image (Fig. 1b), the synthesized magnetic nanoparticles have a uniform and semi-spherical morphology. In addition, the FE-SEM images present, in which the average size of  $\text{Fe}_3\text{O}_4$  nanoparticle was 31 to 40 nm. Also, the FE-SEM images showed that the external surface of magnetic nanoparticles is enough rough to provide more available active sites for improving the catalytic reaction for the degrading of dye molecules. [1,17]. EDS analysis of  $\text{Fe}_3\text{O}_4$  nanoparticles presents some peaks, which related to the Fe and O. These results indicated the magnetic  $\text{Fe}_3\text{O}_4$  has been successfully synthesized in an appropriate form (Fig. 1c).

In addition, the FTIR spectra of  $\text{Fe}_3\text{O}_4$  nanoparticles is shown in Fig. 2. The FTIR spectroscopy is illustrated some adsorption peaks, which were  $3,429$ ;  $1,608$  and  $537 \text{ cm}^{-1}$ . The clear peaks at  $3,429$  and  $1,608 \text{ cm}^{-1}$  are related to the O–H stretching vibration and H–O–H bending, respectively. Also, the peak of  $537 \text{ cm}^{-1}$  could be associated with Fe–O bonds [1,19].

The surface analysis of the  $\text{Fe}_3\text{O}_4$  nanoparticles was carried out with BET analysis. This analysis was done using the adsorption–desorption method by  $\text{N}_2$  which the results of them are shown in Table 1. The specific area of magnetic  $\text{Fe}_3\text{O}_4$  nanoparticles ( $a_s$ ) was  $36.07 \text{ m}^2/\text{g}$ . Adsorption/desorption isotherm of  $\text{N}_2$  on  $\text{Fe}_3\text{O}_4$  nanoparticles and Barrett–Joyner–Halenda (BJH) pore size distribution is shown in Fig. 3a. The image and results of BET analysis (Table 1) could be presented in the presence of a hysteresis loop and mesoporous structure according to the International Union of Pure and Applied Chemistry category [20]. VSM analysis could present the magnetic characteristic of obtained  $\text{Fe}_3\text{O}_4$  nanoparticles. The magnetization curve of synthesized nanoparticles is shown in Fig. 3b. Based on the results, the saturation magnetization of synthesized  $\text{Fe}_3\text{O}_4$  nanoparticles in this study was reported to be about  $50 \text{ emu/g}$ . Furthermore, no remanence, coercivity, and magnetic hysteresis loop indicated that  $\text{Fe}_3\text{O}_4$  had super-paramagnetic properties and could be separated from the solution with an external magnet [1].

### 3.2. Isotherm and kinetic of adsorption

The adsorption experiments were employed before the oxidative tests due to the determination of the adsorption process on the dye removal, achieve the equilibrium time of SSY adsorption onto magnetic  $\text{Fe}_3\text{O}_4$  nanoparticles. The results of the adsorption study at various contact time for the SSY adsorption is shown in Fig. 4. According to the obtained results, the maximum adsorption occurred at an initial 30 min and then reached the equilibrium at 60 min. In other words, at the first stages of the reaction, there is a great number of active adsorption sites on the surface of the adsorbent, but these active sites may be saturated after 30 min by dye molecules and the equilibrium condition of the process has been observed [1,20]. In addition, isotherm and kinetic studies were carried out to explain the interactive behavior of the  $\text{Fe}_3\text{O}_4$  nanoparticles and SSY, anticipate the

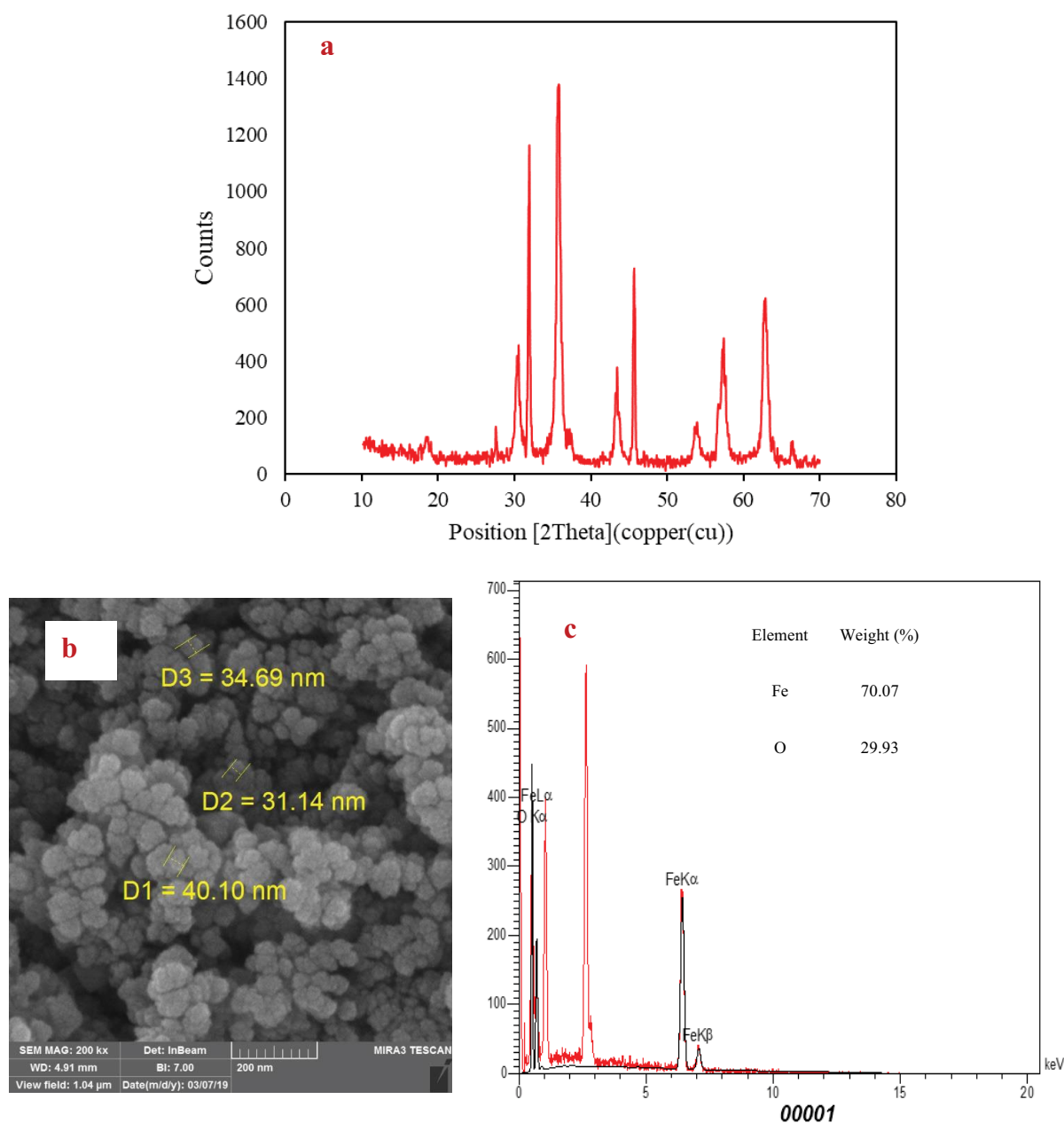


Fig. 1. (a) XRD pattern, (b) FE-SEM analysis, and (c) EDS of synthesized magnetic Fe<sub>3</sub>O<sub>4</sub> nanoparticle.

capacity of adsorbent, modeling, and designing the reactions in the reactor. These studies also prepared further information related to the adsorption mechanism of SSY onto Fe<sub>3</sub>O<sub>4</sub> nanoparticles which are required for predicting the rate of adsorption of the SSY onto adsorbent [21,22]. Therefore, the most important of isotherm (Langmuir and Freundlich models) and kinetic (pseudo-first-order and pseudo-second-order models) were evaluated based on the experimental data, which the results of these models are shown in Table 2. Based on the results and correlation coefficient ( $R^2$ ), the Langmuir isotherm can appropriately fit with data obtained from experimental data ( $R^2$ : 0.99). Thus,

this isotherm could employ for determining the capacity of adsorbent and mutual behavior of SSY onto magnetic Fe<sub>3</sub>O<sub>4</sub> nanoparticles [23]. According to the Langmuir model, the adsorption capacity was 58.1 mg/g which shows dye molecules could be adsorbed moderately on the Fe<sub>3</sub>O<sub>4</sub> nanoparticles. On the other hand, the experimental data adherence significantly to the pseudo-second-order kinetic model ( $R^2$ : 0.98) to describe the rate of reaction and also uses for designing and modeling the reaction occurred in the reactor [22,24]. Moreover, the experimental  $q_e$  was closer to the calculated  $q_e$  obtained from the pseudo-second-order kinetic model, which indicates the results of the kinetics and

accuracy of the modeling. Also, the pseudo-second-order kinetic model could resound the mechanism of the adsorption process was chemisorption and exchange the electron between  $\text{Fe}_3\text{O}_4$  nanoparticles and SSY.

### 3.3. Effect of experimental parameters

#### 3.3.1. Effect of pH of the solution

Solution pH could influence the characteristics of contaminants, the surface of the adsorbent or catalysts, the reaction rate and activity also solubility of the oxidant and ionization of the oxidants and contaminants. Therefore, this parameter can affect the removal efficiency of heterogeneous catalytic degradation of the organic compounds and dye molecules [25]. The results of the effect of solution pH on the removal of SSY is shown in Fig. 5a. In light of the figure, the decolorization efficiency of the  $\text{Fe}_3\text{O}_4/\text{PS}/\text{US}$  system was very fast and decreased critically with an increase in pH. As, the removal efficiency of SSY was significantly decreased from 90.5% to 42.4%, when the pH enlarged

from 3 to 10, respectively. At high pH, more degradation of SSY occurred at the first 30 min and final removal was at 120 min. The SSY and persulfate agents are as negative ion at the aqueous solution, therefore alkaline pH could have a negative effect on the surface charge of activator. This phenomenon could prevent the interaction of magnetic  $\text{Fe}_3\text{O}_4$  nanoparticle and SSY and oxidant agent and then decrease in the generation of active radicals and removal efficiency of pollutants. Furthermore, a non-radical pathway of persulfate through the self-dissociation process would increase at alkaline pH and consequently result in the reduction of degradation of dye molecules [22,26].

#### 3.3.2. Effect of $\text{Fe}_3\text{O}_4$ dosage

Catalyst dosage and active sites on the catalysts could have a significant effect on the degradation of pollutants through catalytic oxidation. More dosage and active sites could make a further available surface for oxidation agents to decomposed and generation of radical and then improve the degradation of pollutants [27]. Furthermore, a high amount of catalysts could lead to an increase in the adsorption rate of SSY molecules on the surface of the  $\text{Fe}_3\text{O}_4$  nanoparticles, and then the degradation rate of SSY enhanced via surface reactions. The results of  $\text{Fe}_3\text{O}_4$  dosage as a catalyst for the degradation of SSY (Fig. 5b) present this phenomenon.

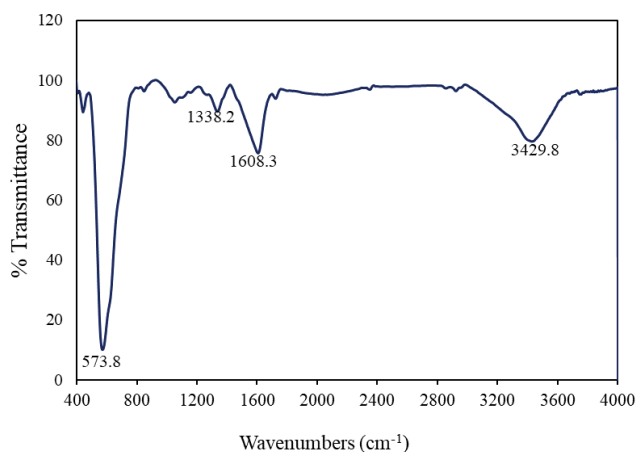


Fig. 2. FTIR of the synthesized  $\text{Fe}_3\text{O}_4$  for dye degradation.

Table 1

BET analysis of magnetic  $\text{Fe}_3\text{O}_4$  nanoparticles for dye removal

Parameters	Value
$V_m$ ( $\text{cm}^3$ (STP) $\text{g}^{-1}$ )	8.2886
$a_{s,\text{BET}}$ ( $\text{m}^2$ $\text{g}^{-1}$ )	36.076
C	120.93
Total pore volume ( $p/p_0 = 0.990$ ), ( $\text{cm}^3$ $\text{g}^{-1}$ )	0.2139
Mean pore diameter (nm)	23.714
Pore structure	Mesopore

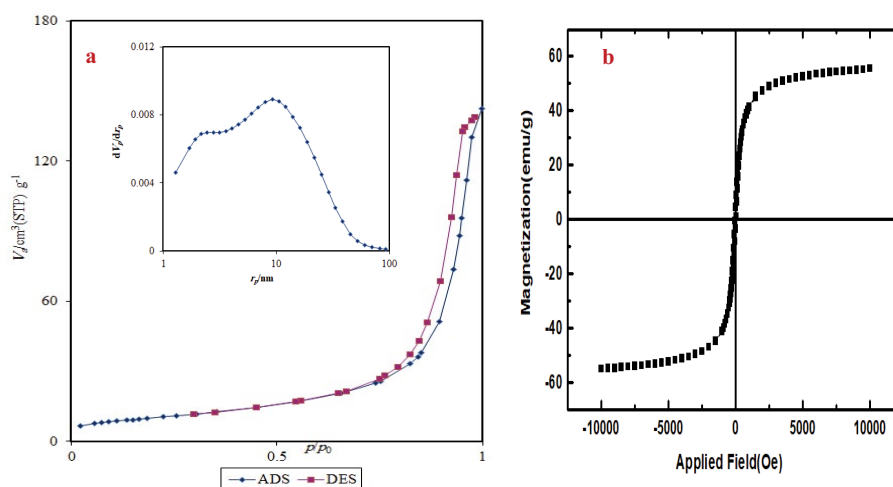


Fig. 3. (a) Adsorption/desorption isotherm of  $\text{N}_2$  on  $\text{Fe}_3\text{O}_4$  nanoparticles (insert: BJH pore size distribution) and (b) VSM image for  $\text{Fe}_3\text{O}_4$  nanoparticles for dye degradation.

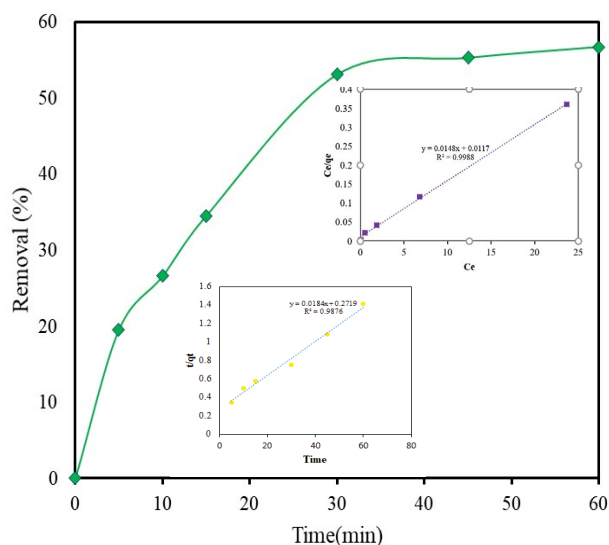


Fig. 4. Results of adsorption studies in removal of SSY (pH: 5; dye concentration: 30 mg/L;  $\text{Fe}_3\text{O}_4 = 0.4$  g/L).

It can be observed that the degradation and reaction rate of SSY accelerated with an increase in catalyst dose [28]. The degradation of SSY increased from 52.8% to 90.5%, as catalyst dosage increase from 0.2 to 0.4 g/L, respectively. However, it can be seen that when the catalyst dosage was enhanced from 0.4 to 0.6, the degradation of SSY decreased from 90.5% to 82%, respectively. The reason for that could be the production of aggregates (self-binding of catalyst magnetic nano-particles), recombination of sulfate radical at a high dosage of catalysts, and the reaction between extra catalysts and sulfate radical according to Eq. (6) [3,22].



In addition, the presence of a further amount of  $\text{Fe}^{2+}$  ions could cause to occur the scavenging circumstance of hydroxyl radicals at high catalyst dosage and reduction of

the excessive number of reactive radicals without reaction with SSY molecules. These reasons could cause to decrease in the degradation of SSY removal at a high dosage of magnetic nanoparticles [1].

### 3.3.3. Effect of dye concentration

The concentration of dye could highly affect the degradation efficiency of magnetic  $\text{Fe}_3\text{O}_4$  nanoparticles/PS concentration. Degradation of a high concentration of dye molecules at aqueous solution needs a high number of free radicals, which could be achieved at a high concentration of persulfate agents. The effect of dye concentration (5–50 mg/L) on the degradation of SSY molecules is shown in Fig. 5c. Based on the results, a high concentration of SSY had a low degradation rate at constant catalyst and PS concentration. This was due to a low amount of persulfate and hydroxyl radical available for the degradation of dye molecules [3,29].

### 3.3.4. Effect of PS concentration

The results of various concentration of persulfate agent on the removal of SSY is shown in Fig. 5d. It can be observed from Fig. 5d, which the degradation rate of SSY molecules at initial times with the increase in PS concentrations from 0.5 to 4 mM sharply was increased and from 79.1% reached 97.4%. However, as PS concentration increased from 4 to 6 mM the degradation rate of SSY molecules was decreased and reached 95.6%. The high concentration of persulfate as a source of produced free radicals of sulfate in the US/ $\text{Fe}_3\text{O}_4$ /PS process could generate a high number of sulfate radicals [30]. Anyway, the sulfate and hydroxyl radicals would be consumed at an excess amount of persulfate concentration through following Eqs. (7)–(9):

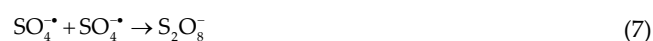


Table 2  
Results of adsorption isotherm and kinetic models used in the study

Isotherm/kinetic type	Equation	Constants	Value
Freundlich	$q_e = K_f C_e^{1/n}$	$K_f$ (mg/g(L/mg) <sup>1/n</sup> )	30.1
		$n$	3.4
		$R^2$	0.958
Langmuir	$q_e = \frac{Q_m K_L C_e}{1 + K_L C_e}$	$Q_m$ (mg/g)	67.56
		$K_L$ (L/mg)	1.26
		$R^2$	0.998
Pseudo-first-order	$\frac{dq_t}{dt} = k_1 (q_e - q_t)$	$q_{e,cal}$ (mg/g)	46.7
		$k_1$ (min <sup>-1</sup> )	0.0024
		$R^2$	0.983
Pseudo-second-order	$\frac{dq_t}{dt} = k_1 (q_e - q_t)^2$	$q_{e,cal}$	54.34
		$K_2$ (g/mg)(min) <sup>-1</sup>	0.0012
		$R^2$	0.988

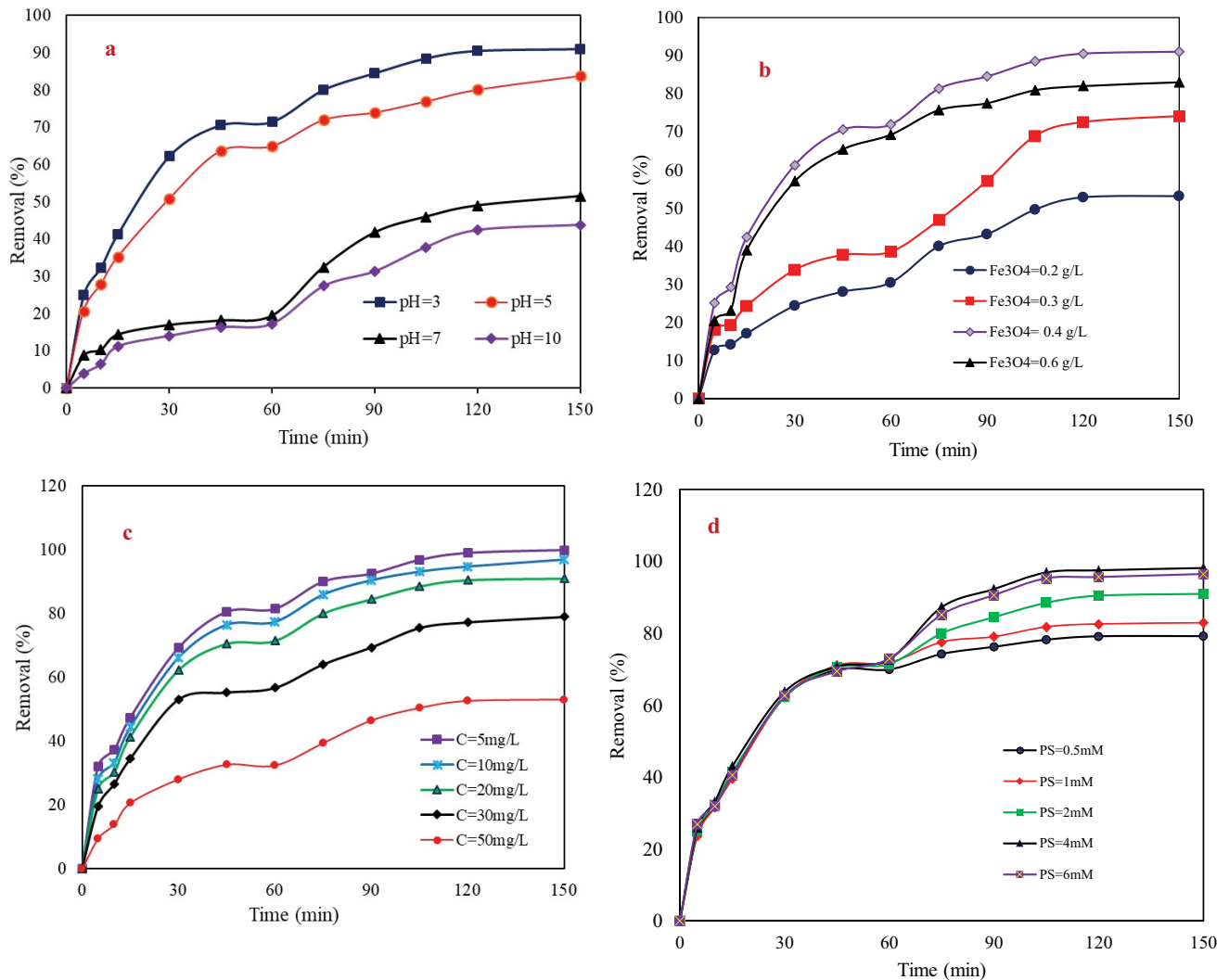


Fig. 5. (a) Effect of pH (dye concentration: 20 mg/L; Fe<sub>3</sub>O<sub>4</sub> = 0.4 g/L; PS: 2 mM; US: 200), (b) effect of catalyst dose (dye concentration: 20 mg/L; pH: 3; PS: 2 mM; US: 200), (c) effect of dye concentration (Fe<sub>3</sub>O<sub>4</sub> = 0.4 g/L; pH: 3; PS: 2 mM; US: 200), and (d) effect of PS concentration (Fe<sub>3</sub>O<sub>4</sub> = 0.4 g/L; pH: 3; dye concentration: 20 mg/L; US: 200).

On the other hand, the number of active sites on the catalyst is another limiting factor. When the amount of catalyst was fixed, the number of active sites could be determined by the amount of radical generated [26,31].

### 3.4. Comparison between Fe<sub>3</sub>O<sub>4</sub>/PS/US and Fe<sub>3</sub>O<sub>4</sub>/H<sub>2</sub>O<sub>2</sub>/US

In order to evaluate the decolorization rate of SSY in the process used in this study and Fe<sub>3</sub>O<sub>4</sub>/H<sub>2</sub>O<sub>2</sub>/US process, the experiments conducted at fixed pH and initial dye concentration. The results of the comparison between Fe<sub>3</sub>O<sub>4</sub>/PS/US and Fe<sub>3</sub>O<sub>4</sub>/H<sub>2</sub>O<sub>2</sub>/US processes for dye molecules degradation is shown in Fig. 6. The results of this comparison showed that the degradation rate of both processes was closed to each other; however, the decolorization rate of Fe<sub>3</sub>O<sub>4</sub>/PS/US (98.5%) was a little more than Fe<sub>3</sub>O<sub>4</sub>/H<sub>2</sub>O<sub>2</sub>/US process (96.8%). This means that a persulfate oxidant could be considered as an efficient agent for the degradation of organic compounds [1,30].

### 3.5. Effect of various anions on the decolorization of SSY

Effect of various anions including nitrate, sulfate, chloride, and carbonate for simulation of real wastewater has been investigated on the decolorization rate of Fe<sub>3</sub>O<sub>4</sub>/PS/US process at optimum condition. The results of various anion effects (with a concentration of 10 mM) on this process are shown in Fig. 7. It can be seen that the effect of carbonate and sulfate anions was much higher than chloride and nitrate. The decolorization rate of Fe<sub>3</sub>O<sub>4</sub>/PS/US process in the presence of nitrate, chloride, sulfate, and carbonate was 97.7%, 95.7%, 88%, and 75.15%, respectively. Anions could act as a radical scavenger and compete with anion dye molecules and convert to the weaker form of radicals such as Cl<sub>2</sub><sup>•-</sup>. But the effect of carbonate was much more than other anions due to increasing the pH of the solution and the decreasing the oxidation potential of agents as mentioned above [32]. The reaction between sulfate and hydroxyl radicals and carbonate anion could lead to producing the

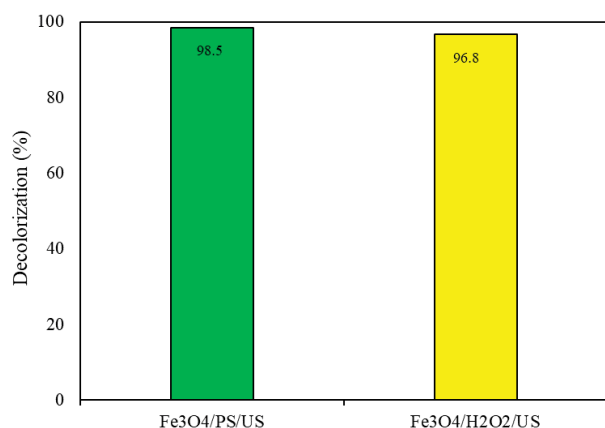


Fig. 6. Comparison between Fe<sub>3</sub>O<sub>4</sub>/PS/US and Fe<sub>3</sub>O<sub>4</sub>/H<sub>2</sub>O<sub>2</sub>/US (Fe<sub>3</sub>O<sub>4</sub> = 0.4 g/L; pH: 3; dye concentration: 20 mg/L; US: 200, PS, and H<sub>2</sub>O<sub>2</sub> = 4 mM).

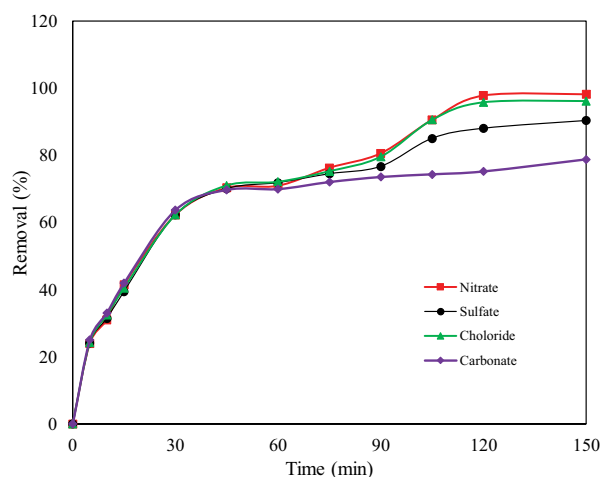


Fig. 7. Effect of various anion competition concentration (Fe<sub>3</sub>O<sub>4</sub> = 0.4g/L; pH: 3; dye concentration: 20 mg/L; US: 200; PS: 4 mM).

radicals of CO<sub>3</sub><sup>•</sup> and HCO<sub>3</sub><sup>•</sup> which are less active than sulfate and hydroxyl radicals. The chloride could react with hydroxyl, sulfate radical, and generate free chlorine radicals, which are weaker radicals than sulfate and hydroxyl. In addition, anions could be adsorbed on the catalyst surface and occupied the active sites. Therefore, anions could act as a scavenger, occupy the active sites of catalysts, and increase the pH of the solution, and finally decrease the degradation rate of the process [1].

### 3.6. Effect of scavenger

Ethanol was used as a scavenger agent for detecting the free radical at Fe<sub>3</sub>O<sub>4</sub>/PS/US process for dye degradation at optimum conditions. Fig. 8 can depict the effect of ethanol as a scavenger with a concentration of 10 mM on the SSY degradation with Fe<sub>3</sub>O<sub>4</sub>/PS/US process. As seen, the degradation of SSY molecules declined as ethanol as a scavenger was added to the solution. The decolorization rate of SSY

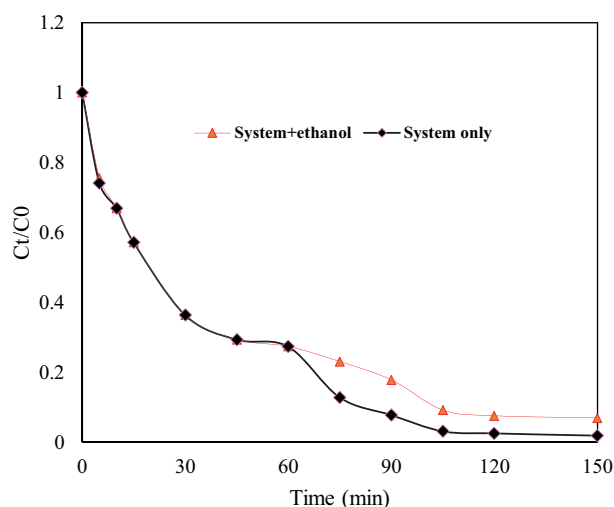


Fig. 8. Effect of scavenger (Fe<sub>3</sub>O<sub>4</sub> = 0.4 g/L; pH: 3; dye concentration: 20 mg/L; PS: 4 mM).

decreased from 97.4% to 92.4% when scavenger was added to the solution of reaction over the 120 min. This means that Fe<sub>3</sub>O<sub>4</sub> could adsorb persulfate agents and generate the sulfate and hydroxyl radicals (heterogeneous reactions) and the reaction between Fe<sup>3+</sup> and persulfate molecules in the solution could also produce the free radicals (homogeneous reactions) [1,33]. These phenomena might accelerate the generation of free radicals and then reaction between dye molecules and radicals and improve the decolorization rate of solution. In addition, trivalent iron could react with the excess amount of persulfate and generate the divalent iron and less reactive radicals such as O<sub>2</sub><sup>•</sup> and HO<sub>2</sub><sup>•</sup> and decrease the degradation rate of dye molecules [34].

### 3.7. Synergistic effect

The comparison between the efficiency of the various process was carried out through some experiments as a control test and the synergetic effect of different processes was determined. Thus, the removal efficiency of the combined process (Fe<sub>3</sub>O<sub>4</sub>/PS/US) was compared with individual processes at the same conditions and the synergetic effect was calculated with Eq. (10) [35]:

$$R = \frac{\text{SSY removed with combined process}}{\text{SSY removed with sum of individual process}} \quad (10)$$

where  $R$  represents the enhancement factor. The enhancement factor ( $R$ ) higher than 1 indicates that the synergetic effect takes place in the process and  $R$ -value less than 1 represents that the antagonistic effect could have occurred in the study Fig. 9, clearly shows the degradation of SSY molecules with various processes at the same conditions. As seen, the decolorization of the US and PS alone was minimum lower than other processes. This means that persulfate and the US alone could not degrade the dye molecules. However, the removal efficiency of magnetic Fe<sub>3</sub>O<sub>4</sub> alone was 71.1%, which mainly is related to the adsorption process. The decolorization rate of Fe<sub>3</sub>O<sub>4</sub>/PS and zerovalent

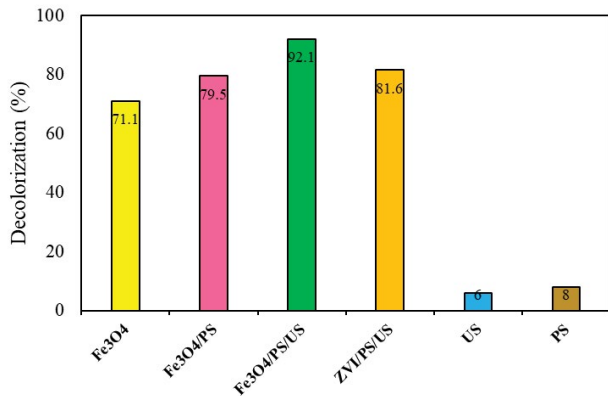


Fig. 9. Control of different process ( $\text{Fe}_3\text{O}_4 = 0.4 \text{ g/L}$ ; pH: 3; dye concentration: 20 mg/L; PS: 2 mM; ZVI: 0.4 g/L).

iron (ZVI)/PS/US process was 79.5% and 82.6%, respectively. This means that the removal efficiency of the  $\text{Fe}_3\text{O}_4$ /PS/US process was significantly higher than both other processes. The comparison between different processes could disclose that degradation and the adsorption process removed concurrently with the organic molecules in this process. Therefore, it could have resulted in adsorption capacity of adsorbent that could directly affect the removal and degradation rate of contaminants through adsorption of oxidation agents and adsorbate. Nevertheless, the enhancement factor ( $R = 1.08$ ) indicated that the synergistic effect occurred at the system and catalytic activity can critically affect the removal rate of SSY [22,35].

### 3.8. Reusability and stability tests

The stability and reusability of the catalyst at various conditions is one of the important factors for using that catalyst. In order to evaluate the reusability and stability factor of  $\text{Fe}_3\text{O}_4$  nanoparticle as a catalyst, the experiments were repeated for four consecutive tests at optimum conditions with no chemical additives. The results of the reusability and stability of the catalyst used in this study shown in Fig. 10. As seen, the catalytic activity of  $\text{Fe}_3\text{O}_4$  was decreased after four cycles and the efficiency of the removal of SSY reached 32.2%. This may be because destroying of active sites on the surface of catalyst with consecutive washing and drying, which cause blocking pores of catalyst surface and reduction of active sites available on the magnetic  $\text{Fe}_3\text{O}_4$  nanoparticles [1,22]. In addition, the stability tests were carried out with measuring the leaching of iron in the aqueous solution at acidic conditions (HCl, 1 M). The results showed that the amount of iron leaching was insignificant and magnetic  $\text{Fe}_3\text{O}_4$  nanoparticles could not generate the secondary pollutant in the aqueous solution [22].

### 3.9. Mineralization tests

The mineralization of SSY molecules in the  $\text{Fe}_3\text{O}_4$ /PS/US system could be determined with the change of TOC values. The results of the mineralization of SSY is shown in Fig. 11. Based on the obtained results, the TOC removal was

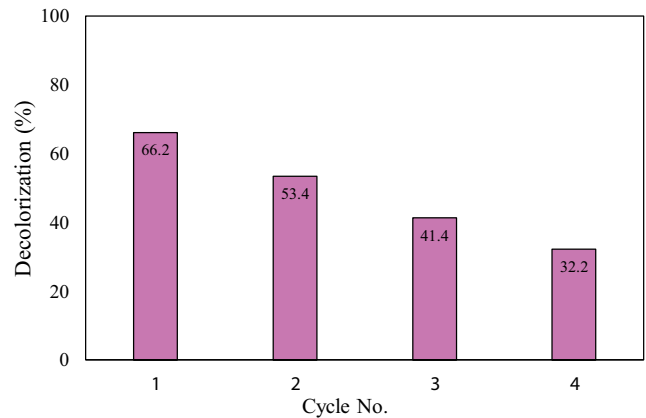


Fig. 10. Recovery ( $\text{Fe}_3\text{O}_4 = 0.4 \text{ g/L}$ ; pH: 3; dye concentration: 20 mg/L; PS: 4 mM).

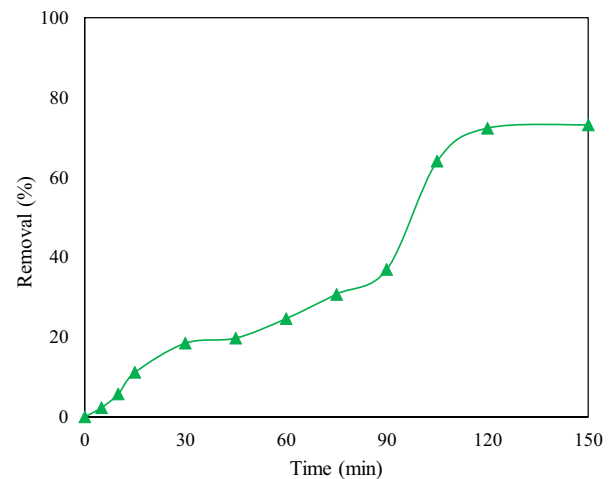


Fig. 11. TOC removal efficiencies by  $\text{Fe}_3\text{O}_4$ /US/PS process ( $\text{Fe}_3\text{O}_4 = 0.4 \text{ g/L}$ ; pH: 3; dye concentration: 20 mg/L; PS: 4 mM).

72.3% after 120 min of reaction. This means that  $\text{Fe}_3\text{O}_4$ /PS/US system could significantly degrade the SSY molecules, but about one-third of intermediates are resistant to degradation and need much more time for mineralization. It was found in previous studies [36].

## 4. Conclusions

Degradation of SSY as an azo dye was conducted in the heterogeneous  $\text{Fe}_3\text{O}_4$ /PS/US system. In this system, magnetic  $\text{Fe}_3\text{O}_4$  nanoparticles could act as both adsorbent and catalyst of persulfate agents and generate sulfate and hydroxyl radicals for degrading the dye molecules onto environmentally friendly compounds. Dye molecules could completely remove from aqueous solution with  $\text{Fe}_3\text{O}_4$ /PS/US system and more than two-thirds of dye molecules mineralized at optimum conditions. The utilization of the catalyst at various conditions showed that the catalyst has good reusability and stability for degrading the SSY to inorganic compounds. The value of the enhancement factor ( $R$ ) represented that the

synergetic effect occurred at the system and  $\text{Fe}_3\text{O}_4$  nanoparticles can be used as an efficient heterogeneous catalyst in the oxidation process for degradation of dye molecules. The effect of competitive anions showed that carbonate ions had more effect on dye degradation due to increasing the pH of the solution and decreasing the oxidation potential of agents.

### Acknowledgment

The financial supports of the present work were provided by the Environmental Technologies Research Center, Ahvaz Jundishapur University of Medical Sciences (Project number: ETRC-9640).

### References

- [1] B. Kakavandi, A. Takdastan, S. Pourfadakari, M. Ahmadmazzam, S. Jorfi, Heterogeneous catalytic degradation of organic compounds using nanoscale zero-valent iron supported on kaolinite: mechanism, kinetic and feasibility studies, *J. Taiwan. Inst. Chem. Eng.*, 96 (2019) 329–340.
- [2] A.K. Mishra, T. Arockiadoss, S. Ramaprabhu, Study of removal of azo dye by functionalized multi walled carbon nanotubes, *J. Chem. Eng.*, 162 (2010) 1026–1034.
- [3] Y.Q. Leng, W.L. Guo, X. Shi, Y.Y. Li, A. Wang, F.F. Hao, L.T. Xing, Degradation of Rhodamine B by persulfate activated with  $\text{Fe}_3\text{O}_4$ : effect of polyhydroquinone serving as an electron shuttle, *J. Chem. Eng.*, 240 (2014) 338–343.
- [4] R. Bibi, M. Arshad, H.N. Asghar, Optimization of factors for accelerated biodegradation of reactive Black-5 azo dye, *Int. J. Agric. Biol.*, 14 (2012) 353–359.
- [5] Y. Anjaneyulu, N.S. Chary, D.S.S. Raj, Decolourization of industrial effluents – available methods and emerging technologies – a review, *Rev. Environ. Sci. Biotechnol.*, 4 (2005) 245–273.
- [6] M. Solís, A. Solís, H.I. Pérez, N. Manjarrez, M. Flores, Microbial decolouration of azo dyes: a review, *Process Biochem.*, 47 (2012) 1723–1748.
- [7] D. Bhatia, N.R. Sharma, J. Singh, R.S. Kanwar, Biological methods for textile dye removal from wastewater: a review, *Crit. Rev. Env. Sci. Technol.*, 47 (2017) 1836–1876.
- [8] J.L. Ge, Y.F. Zhang, Y.-J. Heo, S.-J. Park, Advanced design and synthesis of composite photocatalysts for the remediation of wastewater: a review, *Catalysts*, 9 (2019) 122.
- [9] F. Gholami-Borujeni, A.H. Mahvi, S. Nasser, M.A. Faramarzi, R. Nabizadeh, M. Alimohammadi, Enzymatic treatment and detoxification of acid orange 7 from textile wastewater, *Appl. Biochem. Biotechnol.*, 165 (2011) 1274–1284.
- [10] A. Takdastan, S. Pourfadakari, S. Jorfi, Ultrasonically induced adsorption of nitrate from aqueous solution using  $\text{Fe}_3\text{O}_4$ @activated carbon nanocomposite, *Desal. Water Treat.*, 123 (2018) 230–239.
- [11] S. Rodriguez, L. Vasquez, D. Costa, A. Romero, A.J.C. Santos, Oxidation of Orange G by persulfate activated by Fe(II), Fe(III) and zero valent iron (ZVI), *Chemosphere*, 101 (2014) 86–92.
- [12] X. Wang, L.G. Wang, J.B. Li, J.J. Qiu, C. Cai, H. Zhang, Degradation of Acid Orange 7 by persulfate activated with zero valent iron in the presence of ultrasonic irradiation, *Sep. Purif. Technol.*, 122 (2014) 41–46.
- [13] J. Liu, J.H. Zhou, Z.X. Ding, Z.W. Zhao, X. Xu, Z.D. Fang, Ultrasound irradiation enhanced heterogeneous activation of peroxymonosulfate with  $\text{Fe}_3\text{O}_4$  for degradation of azo dye, *Ultrason. Sonochem.*, 34 (2017) 953–959.
- [14] R. Shokoohi, A. Dargahi, R. Amiri, Z. Ghavami, Evaluation of US/ $\text{S}_2\text{O}_8^{2-}$  compitative process performance in the removal of Erythrosine B dye from aqueous solution, *J. Adv. Environ. Health Res.*, 6 (2018) 1–8.
- [15] H. Kusic, I. Peternel, N. Koprivanac, A. Loncaric Bozic, Iron-activated persulfate oxidation of an azo dye in model wastewater: influence of iron activator type on process optimization, *J. Environ. Eng.*, 137 (2010) 454–463.
- [16] Y. Wei, B. Han, X.Y. Hu, Y.H. Lin, X.Z. Wang, X.L. Deng, Synthesis of  $\text{Fe}_3\text{O}_4$  nanoparticles and their magnetic properties, *Procedia Eng.*, 27 (2012) 632–637.
- [17] P. Loekitowati Hariani, M. Faizal, Ridwan, Marsi, D. Setiabudidaya, Synthesis and properties of  $\text{Fe}_3\text{O}_4$  nanoparticles by co-precipitation method to removal procion dye, *Int. J. Environ. Sci. Dev.*, 4 (2013) 336–340.
- [18] S. Pourfadakari, M. Ahmadi, N. Jaafarzadeh, A. Takdastan, A.A. Neisi, S. Ghafari, S. Jorfi, Remediation of PAHs contaminated soil using a sequence of soil washing with biosurfactant produced by *Pseudomonas aeruginosa* strain PF2 and electrokinetic oxidation of desorbed solution, effect of electrode modification with  $\text{Fe}_3\text{O}_4$  nanoparticles, *J. Hazard. Mater.*, 379 (2019) 120839.
- [19] A. Dalvand, R. Nabizadeh, M.R. Ganjali, M. Khoobi, S. Nazmara, A.H. Mahvi, Modeling of Reactive Blue 19 azo dye removal from colored textile wastewater using L-arginine-functionalized  $\text{Fe}_3\text{O}_4$  nanoparticles: optimization, reusability, kinetic and equilibrium studies, *J. Magn. Magn. Mater.*, 404 (2016) 179–189.
- [20] X.-B. Gong, Degradation of dye wastewater by persulfate activated with  $\text{Fe}_3\text{O}_4$ /graphene nanocomposite, *J. Water Reuse Desal.*, 6 (2016) 553–561.
- [21] Z. Gholami, S.K. Ghadiri, M. Avazpour, M.A. Fard, N. Yousefi, S.S. Talebi, M. Khazaei, M.H. Saghi, A.H. Mahvi, Removal of phosphate from aqueous solutions using modified activated carbon prepared from agricultural waste (*Populus caspica*): optimization, kinetic, isotherm, and thermodynamic studies, *Desal. Water Treat.*, 133 (2018) 177–190.
- [22] N. Yousefi, S. Pourfadakari, S. Esmaeili, A.A. Babaei, Mineralization of high saline petrochemical wastewater using Sono-electro-activated persulfate: degradation mechanisms and reaction kinetics, *Microchem. J.*, 147 (2019) 1075–1082.
- [23] K. Jahangiri, N. Yousefi, S.K. Ghadiri, R. Fekri, A. Bagheri, S.S. Talebi, Enhancement adsorption of hexavalent chromium onto modified fly ash from aqueous solution; optimization; isotherm, kinetic and thermodynamic study, *J. Dispersion Sci. Technol.*, 40 (2019) 1147–1158.
- [24] Z. Bozorgpanah Kharat, M. Mohammadi Galangash, A. Ghavidast, M. Shirzad-Siboni, Removal of reactive black 5 dye from aqueous solutions by  $\text{Fe}_3\text{O}_4$ @ $\text{SiO}_2$ -APTES nanoparticles, *Caspian J. Environ. Sci.*, 16 (2018) 287–301.
- [25] F.X. Chen, S.L. Xie, X.L. Huang, X.H. Qiu, Ionothermal synthesis of  $\text{Fe}_3\text{O}_4$  magnetic nanoparticles as efficient heterogeneous Fenton-like catalysts for degradation of organic pollutants with  $\text{H}_2\text{O}_2$ , *J. Hazard. Mater.*, 322 (2017) 152–162.
- [26] C.-H. Weng, H. Tao, Highly efficient persulfate oxidation process activated with  $\text{Fe}^0$  aggregate for decolorization of reactive azo dye Remazol Golden Yellow, *Arabian J. Chem.*, 11 (2018) 1292–1300.
- [27] S. Sajjadi, A. Khataee, N. Bagheri, M. Kobya, A. Şenocak, E. Demirbas, A.G. Karaoglu, Degradation of diazinon pesticide using catalyzed persulfate with  $\text{Fe}_3\text{O}_4$ @MOF-2 nanocomposite under ultrasound irradiation, *J. Ind. Eng. Chem.*, 77 (2019) 280–290.
- [28] Y. Liu, H.G. Guo, Y.L. Zhang, X. Cheng, P. Zhou, G.C. Zhang, J.Q. Wang, P. Tang, T.L. Ke, W. Li, Heterogeneous activation of persulfate for Rhodamine B degradation with 3D flower sphere-like BiOI/ $\text{Fe}_3\text{O}_4$  microspheres under visible light irradiation, *Sep. Sci. Technol.*, 192 (2018) 88–98.
- [29] M. Ahmadi, J. Behin, A.R. Mahnam, Kinetics and thermodynamics of peroxydisulfate oxidation of Reactive Yellow 84, *J. Saudi Chem. Soc.*, 20 (2016) 644–650.
- [30] K.R. Zhu, H. Xu, C.L. Chen, X.M. Ren, A. Alsaedi, T. Hayat, Encapsulation of  $\text{Fe}^0$ -dominated  $\text{Fe}_3\text{O}_4$ / $\text{Fe}^0$ / $\text{Fe}_3\text{C}$  nanoparticles into carbonized polydopamine nanospheres for catalytic degradation of tetracycline *via* persulfate activation, *Chem. Eng. J.*, 372 (2019) 304–311.
- [31] S. Ahmadi, C.A. Igwegbe, S. Rahdar, The application of thermally activated persulfate for degradation of Acid Blue 92 in aqueous solution, *Int. J. Ind. Chem.*, 10 (2019) 249–260.

- [32] M. Golshan, B. Kakavandi, M. Ahmadi, M. Azizi, Photocatalytic activation of peroxymonosulfate by  $\text{TiO}_2$  anchored on copper ferrite ( $\text{TiO}_2/\text{CuFe}_2\text{O}_4$ ) into 2,4-D degradation: process feasibility, mechanism and pathway, *J. Hazard. Mater.*, 359 (2018) 325–337.
- [33] M.R. Taha, A.H. Ibrahim, Characterization of nano zero-valent iron (nZVI) and its application in sono-Fenton process to remove COD in palm oil mill effluent, *J. Environ. Chem. Eng.*, 2 (2014) 1–8.
- [34] H. Barndök, L. Blanco, D. Hermosilla, Á. Blanco, Heterogeneous photo-Fenton processes using zero valent iron microspheres for the treatment of wastewaters contaminated with 1,4-dioxane, *Chem. Eng. J.*, 284 (2016) 112–121.
- [35] A.D. Shiraz, A. Takdastan, S.M. Borghei, Photo-Fenton like degradation of catechol using persulfate activated by UV and ferrous ions: influencing operational parameters and feasibility studies, *J. Mol. Liq.*, 249 (2018) 463–469.
- [36] H.-Y. Shu, S.-W. Huang, M.-K. Tsai, Comparative study of acid blue 113 wastewater degradation and mineralization by UV/persulfate and UV/Oxone processes, *Desal. Water Treat.*, 57 (2016) 29517–29530.